Microelectronic Engineering 102 (2013) 91–97

Contents lists available at SciVerse ScienceDirect

Microelectronic Engineering

journal homepage: www.elsevier.com/locate/mee

Characterization of transient cavitation in gas sparged solutions exposed to megasonic field using cyclic voltammetry

M. Keswani, S. Raghavan *, P. Deymier

Department of Materials Science and Engineering, The University of Arizona, Tucson 85721, USA

ARTICLE INFO

Article history:
Available online 29 November 2011

Keywords:
Megasonic energy
Transient cavitation
Acoustic streaming
Dissolved gases
Microelectrode
Cyclic voltammetry

ABSTRACT

The application of megasonic energy in semiconductor cleaning solutions has been shown to be very effective in improving the particle removal efficiency (PRE). There has been a significant interest in understanding the phenomena of cavitation and acoustic streaming, which are known to play an important role in particle removal during megasonic cleaning. In the present work, transient cavitation in acoustically (~1 MHz frequency) irradiated aqueous solutions containing different dissolved gases (Ar, N_2 and CO_2) has been characterized with a 25 μm diameter microelectrode using high resolution cyclic voltammetry. Specifically, using ferricyanide as an electrochemical probe, current transients are obtained as a function of time. A simple mathematical analysis based on diffusion is used to correlate the collapse characteristics of a transient cavity to the magnitude of current peaks and the time scale of rise and fall in current.

1. Introduction

Megasonic cleaning is an important technique for removal of particles from wafer surfaces during integrated circuit fabrication [1]. Much of the work in the area of megasonic cleaning has been directed towards understanding the effect of different solution variables such as chemistry and dissolved gas content and sound field parameters such as power density and frequency of the acoustic field on particle removal from surfaces. Of these variables, dissolved gas content can be expected to directly affect gaseous cavitation and therefore is an important parameter for megasonic cleaning.

Several studies have been conducted to identify the role of dissolved gases on particle removal and damage to structures under megasonic conditions [2–7]. These studies have been aimed at investigating the removal of silicon dioxide and silicon nitride particles of different sizes from silicon wafers in chemical solutions irradiated with megasonic energy and containing dissolved gases such as N_2, O_2, He and CO_2. There is considerable discrepancy not only in terms of effect of different dissolved gases on particle removal but also on the mechanism (cavitation or streaming) that is responsible for cleaning. Goh et al. studied the removal of 0.1–1 μm SiO_2 particles from 300-mm silicon wafers in ammonia peroxide mixtures (APM) containing N_2 under megasonic conditions. It was proposed that the increase in particle removal efficiency with increase in dissolved N_2 content from ~2 ppm to 16 ppm was due to microstreaming caused by stable nitrogen bubbles near the wafer surface [2]. In another study, the removal of ~35 nm SiO_2 particles from silicon oxide wafers in degassed de-ionized (DI) water was compared with that in DI water containing 20 ppm of oxygen in a sound field of 0.72 MHz frequency and it was concluded that cavitation and *not* acoustic streaming is responsible for particle removal [4].

Bubble behavior (oscillation and implosion) can be altered by the type and amount of dissolved gas during megasonic exposure and therefore studies have been conducted to characterize bubble activity in solutions containing different gases using techniques based on sonoluminescence measurements and sono-electrochemistry [8,9]. Young was one of the early researchers to relate cavitation intensity to thermal conductivity of dissolved gases [8]. He measured sonoluminescence from 17 different gases (including five inert gases, nitrogen and carbon dioxide) dissolved in DI water that was subjected to 20 kHz of sound frequency at 10 W/cm^2. Although sonoluminescence intensity for inert gases followed an inverse relation with the thermal conductivity of gases, there was no explanation for lower sonoluminescence from carbon dioxide saturated water compared to argon saturated water although both gases have similar values of thermal conductivity.

There has been an increased interest over the past two decades in ultrasonic cavitation studies using microelectrode based electrochemical measurements [10]. This is because microelectrode allows monitoring of single bubble activity through cavitation effects of the bubble that result in enhanced mass transport of the electro-active species at the electrode surface. In one study,

* Corresponding author.
E-mail address: srini@u.arizona.edu (S. Raghavan).

0167-9317/$ - see front matter © 2011 Elsevier B.V. All rights reserved.
doi:10.1016/j.mee.2011.11.013

cyclic voltammetry and chronoamperometry was used to examine the effect of pressure (8–60 bar) on ultrasonic cavitation and acoustic streaming in CO_2 and Ar saturated aqueous solutions [9]. The threshold for cavitation, as determined from the current due to the reduction of hexa-ammineruthenium cation on 25 μm Pt microelectrode, was found to be lower for CO_2 containing solution compared to argon containing solution. The lower cavitation threshold for CO_2 solutions was explained based on higher solubility of the gas compared to argon, a decrease in the interfacial tension of CO_2–water mixture with increase in pressure and the formation of a liquid CO_2 phase under high pressure conditions. Birkin et al. conducted a detailed study on understanding the role of cavitation and acoustic streaming on mass transfer effects in argon saturated aqueous solutions using chronoamperometry and cyclic voltammetry techniques for reduction of hexaammineruthenium on a 6–25 μm microelectrode (C/Pt/Au) [11,12]. Their study revealed that the contribution of cavitation to mass transfer was much higher compared to that of streaming in the ultrasonic frequency range of 20–100 kHz. Although, the current–time peaks were observed to last for a few milliseconds, they were hypothesized to occur due to transient cavitation events that resulted in enhanced mass transfer. More recently, a study on understanding of *single bubble behavior in argon containing aqueous solutions* was conducted using a platinum microelectrode array (ranging from 25 μm to 0.5 mm in diameter) for both ultrasonic (20 kHz) and megasonic (0.5 MHz) frequencies [13,14]. It was shown that at 20 kHz of driving frequency, hemispherical bubbles in the size range of 15 μm–0.8 mm had a life time of several milliseconds. At life times of the order of milliseconds, formation of microjet (which has a life time of a few microseconds or less [15]) was not possible and therefore its occurrence was ruled out. At higher acoustic frequency of 0.5 MHz, current transients were attributed to flux of solution towards the electrode surface due to microstreaming caused by bubble oscillations (~1 μm oscillation amplitude for resonating bubble of 6 μm in size) with life time of tens of milliseconds.

Much of the available literature correlating dissolved gases and bubble behavior is in the ultrasonic frequency range. In the semiconductor industry, cleaning of wafers using acoustic energy is typically carried out at a sound frequency of 1 MHz or higher due to lower damage to structures at these frequencies. Further, there is a potential interest in semiconductor industry to control or reduce transient cavitation in cleaning solutions using dissolved gases. Microelectrode based electrochemical technique offers the advantage of understanding transient cavitation occurring close to a solid surface (the region of interest for wafer cleaning) in comparison to sonoluminescence and hydrophone based techniques that are mainly used for measurements in the bulk of the solution. In the present work high resolution cyclic voltammetry is used to characterize transient cavitation in aqueous solutions containing different dissolved gases (Ar, N_2 and CO_2) and subjected to ~1 MHz sound frequency. Specifically, using ferricyanide as an electrochemical probe, current transients are obtained as a function of time. A simple mathematical analysis based on diffusion is used to correlate the collapse of a transient cavity to the magnitude of current peaks and the time scale of rise and fall in current.

2. Materials and methods

Chemical reagents, potassium ferric cyanide (99.9% $K_3Fe(CN)_6$) and potassium chloride (99.9% KCl) were purchased from Alfa Aesar and were used as received. Platinum wires were of 99.99% purity and purchased from Goodfellow. Aqueous solutions containing 50 mM of $K_3Fe(CN)_6$ and 0.1 M KCl (as supporting electrolyte) were prepared using ultra pure water of resistivity 18 MΩ cm. The solution at 22 ± 2 °C was saturated with a gas (>99% purity) of interest (argon, nitrogen or carbon dioxide) by bubbling the gas in the solution for 30 min. Oxygen removal from solutions was confirmed by measuring the oxygen content using an oxygen sensor (Rosemount Analytical model 499A DO). A gas blanket was maintained over the surface of the solution during experiments to prevent diffusion of atmospheric gases back into the solution.

Electrochemical experiments were performed in the presence and absence of megasonic field using a three-electrode arrangement. A schematic of the electrode set up is shown in Fig. 1. The working electrode used was a 25 μm diameter Pt disk electrode. Platinum wires of diameter 0.05 cm and length 1.0 cm served as counter and pseudo-reference electrode, respectively. All three electrodes were mounted in separate glass (Pyrex®) capillary tubing and affixed in a triangular pattern with ~0.4 cm spacing between them. The back side of each electrode was connected to a copper wire (used as current lead) with a small amount of solder to reduce any stray capacitance. All electrodes were cleaned using iso-propyl alcohol, rinsed thoroughly with DI water, dried with N_2 blow and flame treated prior to each experiment.

All experiments were conducted in a megasonic system provided by ProSys®. The system consisted of a cylindrical polypropylene meg-bowl, 8.9 cm in diameter and 9.5 cm in depth, containing a 1 MHz circular transducer of area 22.2 cm^2 that was covered with sapphire for chemical tolerance. The experiments were run at power densities in the range of 0–2 W/cm^2. The working electrode was positioned close to the center of the transducer at ~2.0 cm above it. A liquid fill height of 2.5 cm was maintained constant in all the experiments.

Cyclic voltammetry experiments were conducted using a Princeton Applied Research potentiostat PARSTAT® 2273 which has a minimum rise time of 0.25 μs, current resolution of 1.2 fA and current sampling rate of ~20 Hz. In all experiments, the scan rate was maintained constant at 0.05 V/s. The temporal variation of current was also recorded using an external oscilloscope (NI USB-5133) at a sampling rate of 0.6 MHz. National Instrument Labview 9.0 was used to acquire and write the data from the oscilloscope, which was processed for graphical output using either MS Excel or DIAdem™ 2010.

3. Results and discussion

Cyclic voltammetry experiments (scan rate of 0.05 V/s) were first conducted in a solution of 50 mM of $K_3Fe(CN)_6$ and 0.1 M KCl saturated with argon gas in the absence and presence of megasonic energy. The results for these measurements at data acquisition rate of 20 Hz are shown in Fig. 2 with the sign convention that the cathodic (reduction) current is negative. In the absence of any sound energy (silent trace (blue color)), as the potential was swept from 0 V to −0.4 V (versus Pt), the magnitude of current increased from 0 to 0.3 μA and then attained a steady value of 0.3 μA (also referred to as limiting current) until the potential reached −0.8 V. No significant current was measured in the positive potential range. The sigmoidal shape of the voltammogram (as opposed to the conventional cyclic voltammogram containing peaks) is due to the microelectrode geometry used in these experiments [12,16]. Application of megasonic field increased the limiting or steady current and also produced current transients riding the baseline current. The steady current value increases from ~0.3 to 0.4 μA with increase in transducer power density from 0 to 2 W/cm^2. This increase in current may be attributed to enhanced mass transport of ferricyanide to the microelectrode or corresponding decrease in diffusion layer caused by convective flow from acoustic streaming [17,13]. The diffusion layer thickness (δ) can be calculated to be ~5.5 and 4.0 μm in the absence and pres-

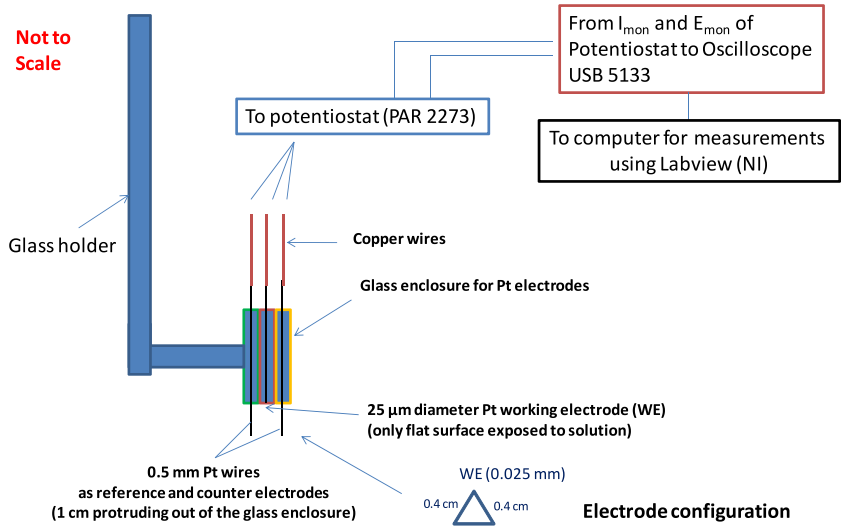

Fig. 1. Schematic of three electrode set up used for electrochemical experiments.

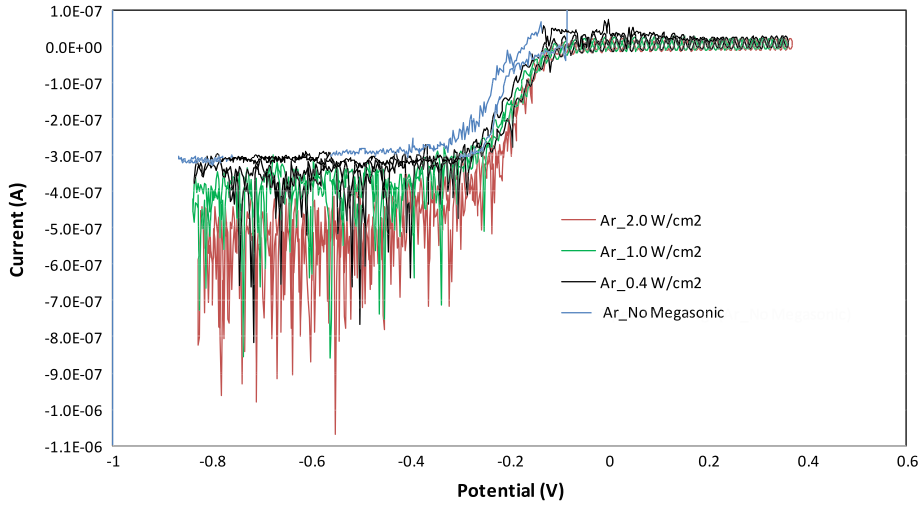

Fig. 2. Cyclic voltammetry results obtained in argon saturated DI water containing 50 mM $K_3Fe(CN)_6$ and 0.1 M KCl solution irradiated with sound of ~1 MHz frequency at different power densities (25 µm WE, scan rate = 0.05 V/s, data acquisition rate = 20 Hz). (*Note:* 7 point moving average was taken for Ar_No megasonic to eliminate the background noise.) (For interpretation of color in this figure, the reader is referred to the web version of this article.)

ence (2 W/cm^2) of megasonic field using the equation $\delta = nFADC_B/I_{lim}$, where I_{lim} is the limiting current, n(=1) is the number of electrons transferred in the reduction of ferricyanide, F is the Faraday constant, D (=0.7 × 10^{-5} cm^2/s [18,19]) and C_B are the diffusion coefficient and bulk concentration of ferricyanide, respectively. It may also be seen from Fig. 2 that the frequency of occurrence and the magnitude of current transients observed during the cathodic scan (−0.2 to −0.8 V) increased with increase in power density.

In order to capture the fine details of the current-transients superimposed on the streaming current, the temporal variation of the current peaks was also measured at a sampling rate of 0.6 MHz. In Fig. 3(a), where the data is shown for megasonic power density of 2 W/cm^2, the gray and red plots correspond to potential and current measured as a function of time, respectively. Comparing the current peaks in Fig. 3(a) with those in Fig. 2, it may be observed that sampling the data at a higher rate reveals additional current peaks. The magnitude of the current peaks ranges up to 1 µA with the highest peak magnitude about three times larger than the steady baseline current under no megasonic condition. Fig. 3(b) shows examples of expanded current transient peaks. The rise and fall times for the currents shown in the top of the figure are ~35 and 100 ms, respectively. Overall, the rise and fall times for various peaks observed during megasonic exposure were found to be in the range of 5–40 ms and 50–120 ms, respectively. The current peaks may be attributed to implosion of transient bubble(s) near the electrode surface, which results in an increase in the concentration of ferricyanide species. Mishra et al. have shown that depending on the fluid velocity due to the collapsing bubble transport of species by advection can lead to significant enrichment/accumulation of the species at the liquid vapor interface [20]. After the collapse, the ferricyanide species start diffusing out radially and as it reaches the electrode surface, the current will change depending on the ferricyanide concentration. The current peak shown in the bottom of Fig. 3(b) exhibits a composite current behavior which could be a result of multiple bubble collapses occurring simultaneously in the proximity of the electrode surface. The shape of current transient data may be used to estimate the distance (r) of the (center of) imploding cavity from the electrode surface. Current is proportional to the concentration of the electro-

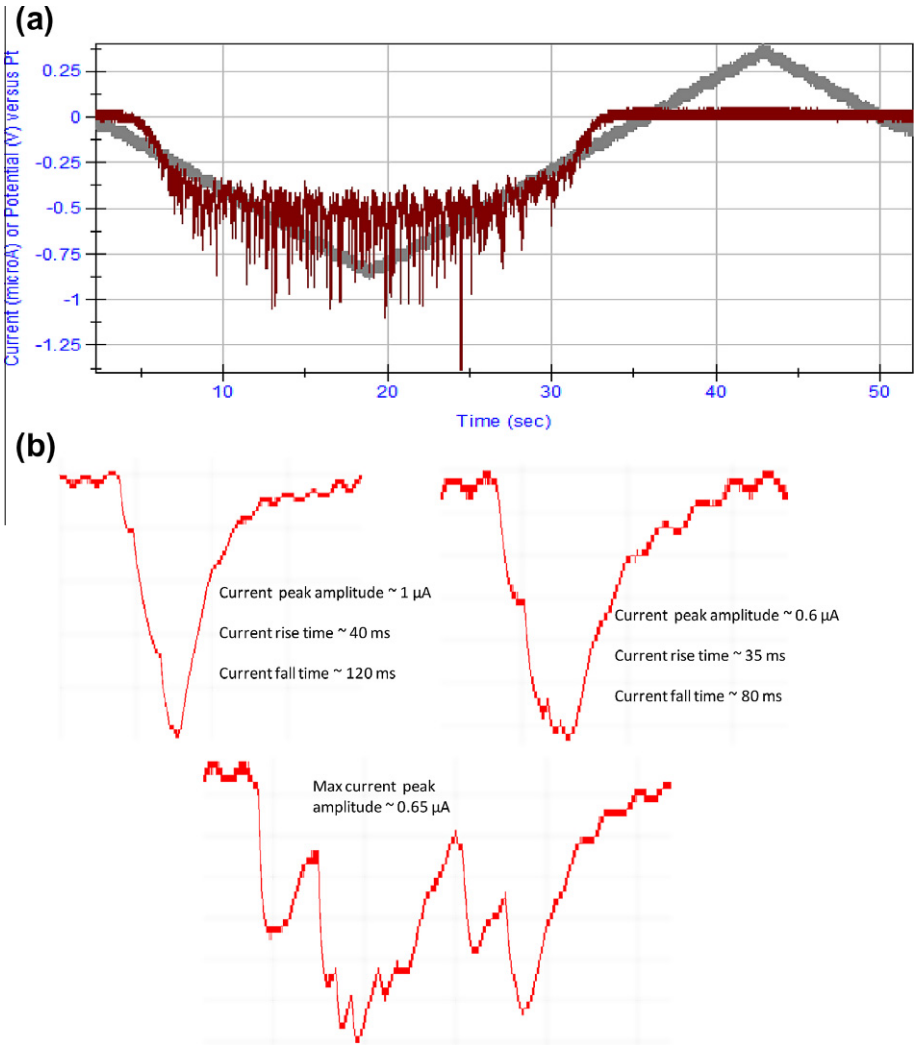

Fig. 3. (a) High resolution (0.6 MHz sampling rate) cyclic voltammetry results obtained in argon saturated DI water containing 50 mM $K_3Fe(CN)_6$ and 0.1 M KCl solution irradiated with sound of ~1 MHz frequency at 2.0 W/cm^2 power density, scan rate = 0.05 V/s. (b) Examples of current transients superimposed on the limiting current obtained for experimental conditions similar to that used to obtain data in (a).

active species at the electrode surface [19,21] and this concentration, which is a function of '*r*' and time, may be calculated using appropriate models. Only for certain '*r*' values, the shape of the concentration versus time data may be expected to match the shape of the transient peak.

The concentration profile for ferricyanide at different times after the collapse of single transient cavity can be obtained by formulating a differential equation and solving it analytically using suitable boundary conditions. The derivation is shown in the appendix but the final equation resulting from this derivation is below Eq. (1):

$$C_A = C_B + \frac{M}{8(\pi D t)^{\frac{3}{2}}} e^{-\frac{r^2}{4Dt}} \tag{1}$$

Eq. (1) relates ferricyanide concentration, C_A, at different radial distances (r) and times (t) to moles of ferricyanide, M, accumulated at the center of the bubble at the end of its collapse. Using Eq. (1), different ferricyanide concentration profiles (C_A versus time) can be generated for a range of values of r, provided M is known. The value of M can be computed as follows. At 1 MHz of sound frequency, bubbles of ~3.5 μm resonant radius (R_o) can be expected to be present in the solution [22]. In order for a bubble of this size to transform into a transient cavity at a megasonic power density of 2 W/cm^2, it must grow to approximately two times its initial size [23] to a maximum radius (R_{max}) of ~7 μm. We assume here that at the end of the collapse, the amount of ferricyanide contained in a liquid volume of radius R_{max} gets accumulated in a small region at the center of the bubble due to advection as highlighted earlier. This assumption may not be unreasonable considering the high bubble velocity and radial compression ratio during the collapse. Since, the initial concentration of ferricyanide (at $t = 0$) is 0.05 M, the value of M can be computed to be $\sim 8 \times 10^{-14}$ mol using R_{max} of 7 μm.

Fig. 4 shows the ferricyanide concentration profiles for different values of r ranging from 2 to 20 μm. In all cases, the concentration of ferricyanide increases with time above its initial value and then drops back to the initial concentration. For $r < 4$ μm, the rise times are lower than 5 ms and also the increase in ferricyanide concentration is five times or larger than the initial concentration. Similarly, for $r > 10$ μm, the increase in ferricyanide concentration is very small (<10%). The concentration profiles for values of r in the range of 5–10 μm exhibit rise times between 5 and 20 ms and fall times of about 100 ms. Additionally, the concentration at the peak is about 1.1–2.0 times larger than the initial concentration. It may be recalled that the measured current peaks were three times or lower in amplitude (or height) compared to the steady current and exhibited rise times of 5–40 ms and fall times of 50–

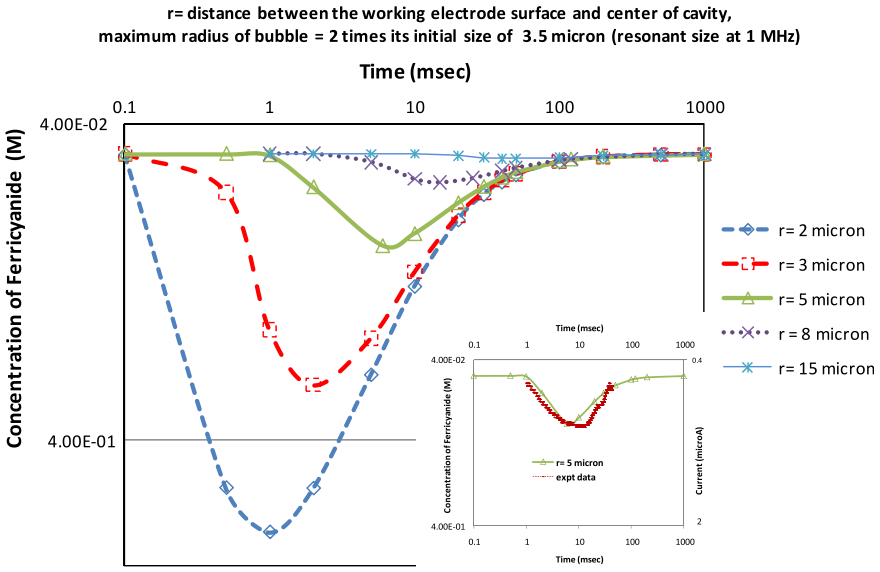

Fig. 4. Concentration–time plots generated for different values of r using an initial bubble radius (R_o) of 3.5 μm. (Inset shows fit of generated data (for r = 5 μm) to the experimental data.)

120 ms. Therefore, it seems that the value of r (distance of the (center of) imploding cavity from the electrode surface) between 5 and 10 μm provides a good fit of calculated concentration–time data with some of the measured current transients (an example shown in the inset of Fig. 4). Implosion of a bubble close to a surface may also give rise to microjetting [24,25]. However, microjetting cannot yield peak shapes shown in Fig. 3(b) for the following reason. With the liquid jet velocity of about 100 m/s and initial bubble radius of 3.5 μm, the duration of impact will be $\sim 10^{-7}$ s. This time scale is many orders of magnitude lower than the rise time of the current peaks measured in our experiments ruling out the current increase due to the jet impact. However, during the jet formation, the collapsing cavities reduce in size considerably [26] leading to significant local enrichment in ferricyanide concentration. While a jet may disperse some of this concentrated solution, diffusion will still be the primary mechanism for the homogenization of the solution after asymmetric bubble collapse.

The effect of dissolved nitrogen and carbon dioxide on transient cavitation in the presence of megasonic field at 2 W/cm^2 is shown in Fig. 5. In the absence of the megasonic energy, the current potential trace (light green and black) is the same as that observed in the case of argon saturated aqueous solution. With the application of acoustic energy at 2 W/cm^2, the limiting current increases to ~0.4 μA with current transients superimposed on it. The increase in limiting current, again attributed to the streaming effect, is independent of the type of dissolved gas. However, the current transients strongly depend on the nature of the dissolved gas. The number and magnitude of current peaks were observed to decrease in the following order for dissolved gases: argon > nitrogen > carbon dioxide. Interestingly, in the case of aqueous solution saturated with CO_2 gas, the current for peak with the highest amplitude was about 10 times lower than the one in argon saturated solution. Overall, the magnitude of current peaks in CO_2 sparged aqueous solution was significantly lower than in Ar sparged aqueous solution. A plot of frequency of occurrence of transient cavitation (#/10 s) with peak current values greater than 0.6 μA as a function of megasonic power density for different dissolved gases (Ar, N_2 and CO_2) is shown in Fig. 6. In the case of Ar saturated ferricyanide solution, the frequency of occurrence of 'current peaks' increases from ~6 to 65 in 10 s with increase in power density from 0.4 to

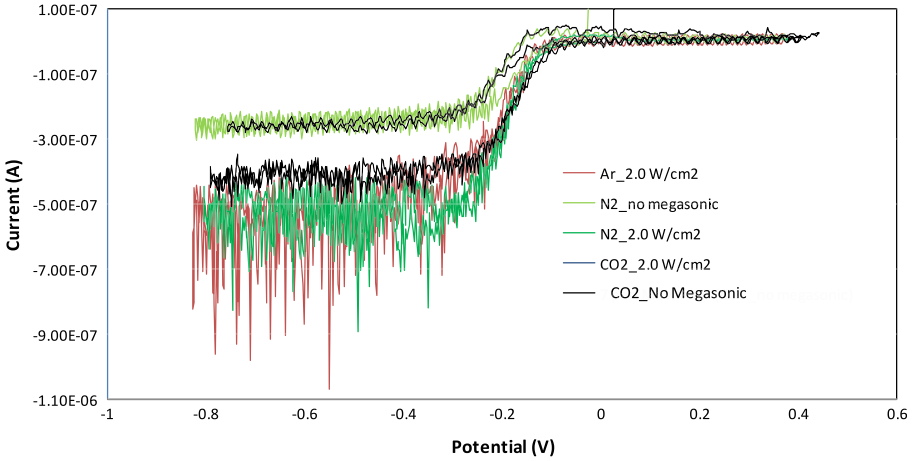

Fig. 5. Effect of dissolved gases (CO_2, N_2 and Ar) in 50 mM $K_3Fe(CN)_6$ and 0.1 M KCl solution on current voltage behavior (~1 MHz sound frequency and 2.0 W/cm^2 power density, 25 μm WE, scan rate = 0.05 V/s, data acquisition rate = 20 Hz. (*Note:* 7 point moving average was taken for CO_2_No megasonic to eliminate the background noise.) (For interpretation of color in this figure, the reader is referred to webversion of this article.)

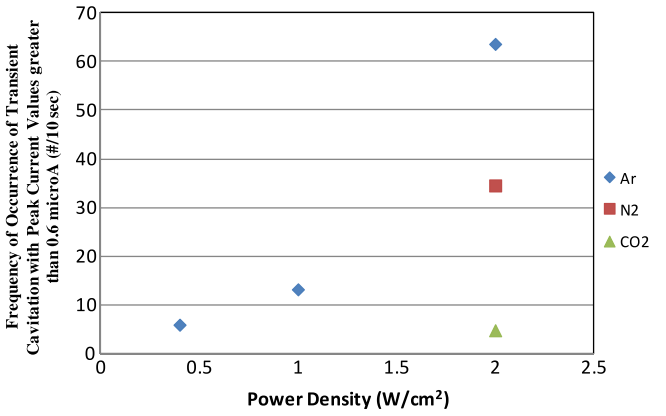

Fig. 6. Frequency of occurrence of transient cavitation (#/10 s) with peak current values greater than 0.6 μA as a function of power density for various dissolved gases.

2 W/cm^2. Interestingly, the number of 'current peaks' at 2 W/cm^2 reduces to 35 and 5 (in 10 s) when the experimental solution contained saturated levels of N_2 and CO_2, respectively.

It may be noted that CO_2 gas has much higher solubility (~1500 ppm) in water compared to N_2 (~18 ppm) and Ar (~55 ppm). Therefore, higher amounts of CO_2 gas can diffuse into the cavity during the expansion phase and can cushion the subsequent collapse. This will result in a lower amount of accumulated ferricyanide at the center of the bubble at the end of its collapse. The reason for lower current peaks in N_2 saturated solution compared to Ar saturated solutions is unknown at this time. These results show that transient cavitation can be controlled by dissolving a suitable gas in the cleaning solution during megasonic cleaning of semiconductor surfaces. The use of dissolved CO_2, in particular, may prove to be beneficial for particle removal from patterned wafers. This is due to the fact that subdued transient cavitation in CO_2 containing solution will potentially reduce feature damage while streaming (including microstreaming) forces may preserve particle removal efficiency (PRE) [27].

4. Conclusions

Transient cavitation was characterized in acoustically (~1 MHz frequency) irradiated solutions containing different dissolved gases (Ar, N_2 and CO_2) using high resolution cyclic voltammetry on a microelectrode. The current peaks obtained using ferricyanide as an electrochemical probe were attributed to diffusion of ferricyanide concentrated at the center of the transient cavity at the end of the implosion. A mathematical model based on diffusion was used to correlate the collapse of a transient cavity to the magnitude of current peaks and the milli-second time scale of rise and fall in current. The number and magnitude of current peaks were observed to decrease in the following order for dissolved gases: argon > nitrogen > carbon dioxide.

Acknowledgements

The authors acknowledge financial support from National Science Foundation (Award ID: 0925340). The authors would also like to thank Mark Beck of Product Systems, Inc. (ProSys) for donation and support of meg-bowl® equipment.

Appendix A

If C_A is the concentration of ferricyanide at a distance r from the center of bubble after its collapse at any time t, then the differential equation in spherical coordinates can be written as:

$$D\frac{\partial}{\partial r}\left(4\pi r^2\frac{\partial C_A}{\partial r}\right)=4\pi r^2\frac{\partial C_A}{\partial t} \tag{A1}$$

where D, the diffusion coefficient of ferricyanide ion, is assumed to be independent of r

$$D\frac{\partial^2 C_A}{\partial r^2}+\frac{2D}{r}\frac{\partial C_A}{\partial r}=\frac{\partial C_A}{\partial t} \tag{A2}$$

Let $\overline{C_A}=C_A-C_B$.

Eq. (A2) now becomes,

$$D\frac{\partial^2 \overline{C_A}}{\partial r^2}+\frac{2D}{r}\frac{\partial \overline{C_A}}{\partial r}=\frac{\partial \overline{C_A}}{\partial t} \tag{A3}$$

Let $u=r\overline{C_A}$.

Eq. (A3) can be written as

$$D\frac{\partial^2 u}{\partial r^2}=\frac{\partial u}{\partial t} \tag{A4}$$

Taking Laplace transform of Eq. (A4)

$$su_L(r,s)-u(r,t=0)=D\frac{\partial^2 u_L(r,s)}{\partial r^2} \tag{A5}$$

At $t=0,\ C_A=C_B,\ \overline{C_A}=0,\ u=0$

$$su_L(r,s)=D\frac{d^2 u_L(r,s)}{dr^2} \tag{A6}$$

Eq. (A6) is an ordinary differential equation and the solution to this equation is:

$$u_L=Ae^{-\sqrt{\frac{s}{D}}r}+Be^{\sqrt{\frac{s}{D}}r} \tag{A7}$$

As $r\to\infty,\ C_A\to C_B,\ \overline{C_A}\to 0,\ u\to 0$ and $u_L\to 0$.

Therefore, B must be zero

$$u_L=Ae^{-\sqrt{\frac{s}{D}}r} \tag{A8}$$

If M is the moles of ferricyanide accumulated at $r=0$ at the end of transient cavity collapse, then

$$M=\int_0^\infty (C_A-C_B)4\pi r^2 dr \tag{A9}$$

$$M=4\pi\int_0^\infty urdr \tag{A10}$$

Taking Laplace transform,

$$\frac{M}{s}=4\pi\int_0^\infty u_L rdr \tag{A11}$$

$$\frac{M}{s}=4\pi\int_0^\infty Ae^{-\sqrt{\frac{s}{D}}r}rdr \tag{A12}$$

After integration by parts,

$$A=\frac{M}{4\pi D} \tag{A13}$$

Therefore,

$$u_L=\frac{M}{4\pi D}e^{-\sqrt{\frac{s}{D}}r} \tag{A14}$$

Taking Laplace Inverse,

$$u=\frac{Mr}{8(\pi Dt)^{\frac{3}{2}}}e^{-\frac{r^2}{4Dt}} \tag{A15}$$

$$C_A=C_B+\frac{M}{8(\pi Dt)^{\frac{3}{2}}}e^{-\frac{r^2}{4Dt}} \tag{A16}$$

References

[1] M. Keswani, S. Raghavan, P. Deymier, S. Verhaverbeke, Microelectronic Engineering 86 (2009) 132–139.

[2] B. Goh, F. Goh, C. Lim, Z. Ismail, M. Zhou, Solid State Phenomena 134 (2008) 217–220.
[3] Y. Hagimoto, K. Asada, H. Iwamoto, IEEE International Symposium on Semiconductor Manufacturing 8624905 (2005) 215–218.
[4] G. Vereecke, E. Parton, F. Holsteyns, K. Xu, R. Vos, P. Mertens, Micro Magazine 22 (2004) 57–63.
[5] G. Vereecke, F. Holsteyns, S. Arnauts, S. Beckx, P. Jaenen, K. Kenis, M. Lismont, M. Lux, R. Vos, J. Snow, P. Mertens, Solid State Phenomena 103–104 (2005) 141–146.
[6] K. Muralidharan, M. Keswani, H. Shende, P. Deymier, S. Raghavan, F. Eschbach, A. Sengupta, Proceedings of the SPIE 65171E (2007).
[7] R. Gouk, J. Blocking, S. Verhaverbeke, 23rd Annual Semiconductor Pure Water and Chemicals Conference (2004) 170–182.
[8] F. Young, Journal of the Acoustics American Society 60 (1) (1976) 100–104.
[9] D. Goldfarb, H. Corti, F. Marken, R. Compton, Journal of Physical Chemistry 102 (1998) 8888–8893.
[10] P. Birkin, D. Offin, T. Leighton, Electrochemistry Communications 6 (11) (2004) 1174–1179.
[11] P. Birkin, C. Delaplace, C. Bowen, Journal of Physical Chemistry 102 (52) (1998) 10885–10893.
[12] P. Birkin, S. Silva-Martinez, Electroanalytical Chemistry 416 (1996) 127–138.
[13] E. Maisonhaute, P. White, R. Compton, Journal of Physical Chemistry B 105 (48) (2001) 12087–12091.
[14] E. Maisonhaute, F. Javier Del Campo, R. Compton, Ultrasonics Sonochemistry 9 (2002) 275–283.
[15] K. Gandhi, R. Kumar, Sadhana 19 (6) (1994) 1055–1076.
[16] M. Tian, X. Jing, Electroanalysis 9 (9) (1997) 718–721.
[17] F. Marken, R. Akkermans, R. Compton, Electroanalytical Chemistry 415 (1996) 55–63.
[18] S. Konopka, B. McDuffie, Analytical Chemistry 42 (14) (1970) 1741–1746.
[19] B. Pollet, J. Hihn, M. Doche, J. Lorimer, A. Mandroyan, T. Mason, Journal of the Electrochemical Society 154 (10) (2007) E131–138.
[20] S. Mishra, P. Deymier, K. Muralidharan, G. Frantziskonis, S. Pannala, S. Simunovic, Ultrasonics Sonochemistry 17 (2010) 258–265.
[21] S. Hwang, Integrated CMOS Microsystems for Electrochemical Sensing (2010).
[22] F. Young, Cavitation, McGraw-Hill, 1989, pp. 48–50.
[23] T. Leighton, The Acoustic Bubble, vol. 10, Academic Press, 1997, p. 324.
[24] M. Plesset, R. Chapman, Journal of the Fluid Mechanics 47 (2) (1998) 283–290.
[25] E. Brujan, G. Keen, A. Vogel, J. Blake, Physics of Fluids 14 (1) (2002) 85–92.
[26] A. Pearson, J. Blake, S. Otto, Journal of Engineering Mathematics 48 (2004) 391–412.
[27] G. Gale, A. Busnaina, Particulate Science and Technology 17 (3) (1999) 229–238.